BULLETIN OF THE POLISH ACADEMY OF SCIENCES
TECHNICAL SCIENCES
DOI: 10.24425/bpasts.2026.158777

The Simulations of Transients in a Shell Transformer with Movable Magnetic Shunt

Bronisław Tomczuk[1], Dawid Wajnert[1], Dawid Weber[2]

[1] Department of Electrical Engineering and Mechatronics, Opole University of Technology, Opole, Poland
[2] Technology Center, Hitachi Energy, Lodz, Poland

Abstract. A hybrid field-circuit model of a single-phase shell-type transformer that incorporates a three-dimensional analysis of the magnetic field in a transformer with beveled edges of the magnetic shunt. The finite element method (FEM) was employed, and the expressions for computing the magnetic field's differential and integral parameters were provided. For various positions of the magnetic shunt, the self- and mutual inductances of the transformer windings are calculated. Their values are stored in matrix form and serve as input data for the transformer circuit model. The differential equations governing the operation of a transformer with a movable magnetic shunt are formulated using Lagrangian methods. They were applied to the transformer's T-type equivalent circuit. This simulation model has been verified experimentally. Comparison of the measured and simulated time-course currents yields a good agreement. Furthermore, three electric arc models have been introduced to assess the applicability of the proposed approach under nonlinear loading. The results confirm that the mathematical model accurately predicts the transformer transients across a range of operating scenarios. Moreover, the presented simulation offers potential for broader application to other electromagnetic objects.

Keywords: Simulation of Voltage and Current Transients, Field-Circuit Models, Finite Element Analysis, Electric Arc models, Transformer with Magnetic Shunt

1. INTRODUCTION

Mathematical models play a significant role in numerous scientific fields [1-3]. They enable simulation and thus understanding, optimization, and prediction in various conditions of phenomena that are too complex for direct study. It is almost impossible to develop a mathematical model of a transformer that accounts for all physical phenomena. Furthermore, the computational time required to solve such a model would make computer simulations of little practical use. Mathematical models are often simplified by making assumptions and omitting phenomena to improve clarity [4], and despite these simplifications, they remain valuable tools in many applications. In the design and analysis of transformer operation, numerical simulations are widely used to analyze the electromagnetic field distributions [4-6]. Commercial software is available that includes two-dimensional and three-dimensional methods, among which the finite element method (FEM) is the most commonly employed [7]. Knowledge of the transformer's electromagnetic field distribution enables the determination of its key parameters already at the design stage of the structure [8-9].

Furthermore, it enables the assessment of how changes to the transformer design affect these parameters [4, 10]. While numerical calculations of the electromagnetic field distribution can provide accurate results, they are always subject to convergence errors. Analytical solutions, on the other hand, are often more challenging to obtain and require simplifying assumptions about the geometry, as well as the introduction of correction factors to account for these assumptions [11].

This field-circuit model enables the calculation of current and voltage time waveforms in the dynamic and steady states of transformer operation. For this purpose, electromagnetic field equations and circuit differential equations are combined to form a system of equations. In each calculation step, equations describing the field part (magnetic field equations) and the circuit part of the model (circuit current and voltage equations) are solved. Solving the field equations allows us to determine the couplings that generate the electromotive force. The equations from the circuit part enable the determination of the currents that generate the magnetic field in the next step of the field part calculations. Performing field-circuit analysis enables reliable simulations, even with highly nonlinear loads, without the need to build expensive prototypes. Examples of solutions for field and field-circuit models of transformers are presented, among others, in the works [12, 13].

The proposed approach differs from traditional field–circuit models in that it does not solve the field equations during circuit simulation. Instead, the field parameters are precomputed once and used directly within the circuit model. This approach can significantly reduce the computational time required to simulate complex electromagnetic systems, such as DC-DC converters,

because the most time-consuming calculations are field simulations that need to be performed only once [14].
In this paper, the proposed model is analyzed using the example of a transformer with a magnetic shunt inserted into its window, as shown in Figure 1. The studied object was selected due to the significant nonlinearity of the leakage inductance caused by the movable magnetic shunt [4] and the nonlinearity of the load, which is an electric arc.

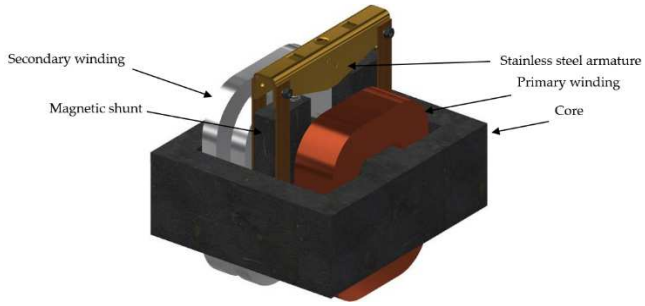

Fig. 1. Three-dimensional outline of the transformer used to verify the proposed mathematical model.

The main dimensions (in millimeters) of the magnetic core and shunt are given in Figs. 2 and 3.

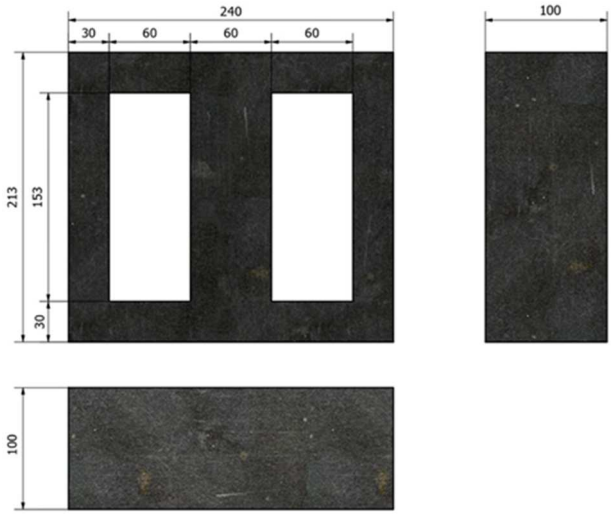

Fig. 2. Dimensions of the magnetic core.

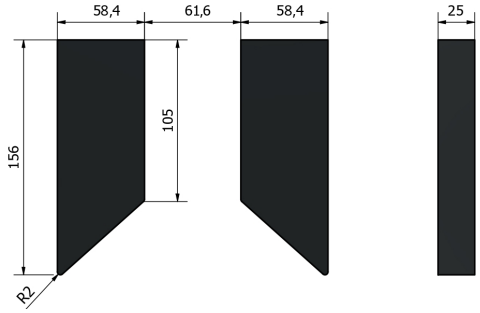

Fig. 3. Dimensions of the magnetic shunt.

The parameters for the analyzed transformer are listed in Tab.1. The winding resistances were determined analytically [8] and are equal to R_1 = 198mΩ and R_2 = 12mΩ, respectively.

TABLE 1. Parameters of the analyzed transformer

Parameter	Value
Rated voltage, V_N	400 [V]
Maximal current of the primary winding, $I_{1\,max}$	40 [A]
Maximal current of the secondary winding, $I_{2\,max}$	225 [A]
Apparent power, S	16 [kVA]
Primary winding resistance, R_1	0,198 [Ω]
Secondary winding resistance, R_2	0,012 [Ω]
Turn number of the primary winding, N_1	180
Turn number of the secondary winding, N_2	34
Material of the magnetic core	M530 - 50A

The magnetic shunt is inserted exactly in the middle of the transformer window. Figs. 4 and 5 present the main dimensions (in millimeters) of the primary and secondary windings.

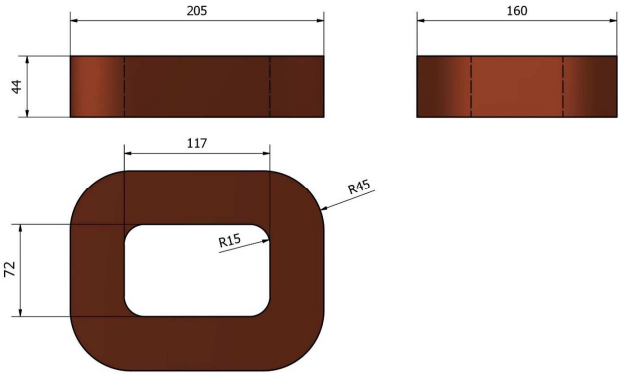

Fig. 4. Dimensions of the primary winding.

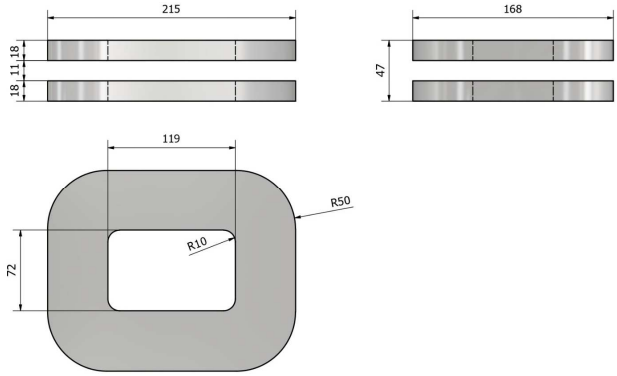

Fig. 5. Dimensions of the secondary winding.

The dynamic leakage inductances of the windings and the mutual inductance were determined based on the analysis of the electromagnetic field distributions. Dynamic inductance values were obtained over the entire B–H curve, enabling more accurate simulation of transient waveforms in the circuit model. The equations of a single-phase transformer were derived using the Lagrange method, and these equations were subsequently used to construct a circuit model capable of simulating the transformer's current and voltage waveforms. The position of the magnetic shunt and the supply voltage of the primary winding can be incorporated into the model. The proposed model was verified by comparing the measured and calculated currents in the transformer's short-circuit state. The model was

also evaluated under nonlinear loads, such as an electric arc. Three different electric arc models were implemented and analyzed.

2. ELECTROMAGNETIC FIELD ANALYSIS

There are many methods for analyzing electromagnetic field distributions, among the most popular are the Finite Difference Method (FDM), the Finite Element Method (FEM), and the Integral Equation Method (IEM) [15, 16]. Electromagnetic field calculations performed in this research take into account the three-dimensional nature of the field, which is implemented in the commercial Maxwell 3D software, where FEM is used. The plane of symmetry [7], in the analyzed transformer's geometry, is presented in Fig. 6.

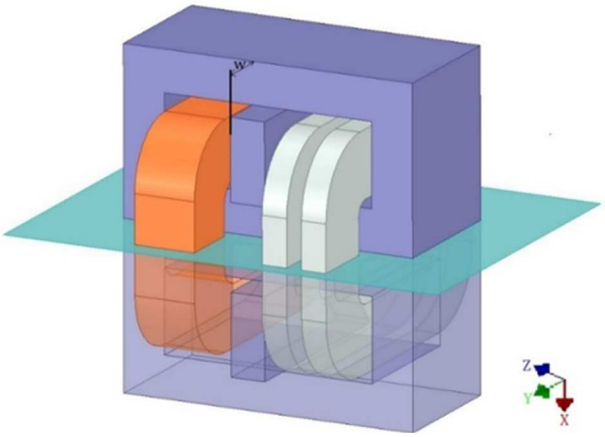

Fig. 6. The symmetry plane in the analyzed transformer geometry.

Knowledge of the magnetic field distribution enables the computation of key integral and differential field parameters. The static leakage inductance L_{rs} can be determined, Eq. (1), using the leakage energy W stored in the non-magnetic regions (Eq. (2)) with magnetic permeability μ, where V is the volume surrounding the magnetic core, and B represents the magnetic flux density in this region.

$$L_{rs} = \frac{2W}{i^2}. \tag{1}$$

$$W = \frac{1}{2\mu}\left(\int_V B^2 dV\right). \tag{2}$$

The dynamic leakage inductance L_{rd} in a linear medium can be determined using the expression provided in Eq. (3) [17, 18].

$$L_{rd} = L_{rs} + I\frac{\partial L_{rs}}{\partial i}. \tag{3}$$

where I is the winding current.

A magnetic shunt inserted into the transformer window divides the flux produced by the primary winding into two parts. One part closes through the magnetic shunt and is not associated with the secondary winding, while the other bypasses the shunt and passes through the secondary winding.

Taking the above into account, the dynamic mutual inductance $L_{\mu d}$ was determined using (Eq. 4) by assuming that only the primary winding is excited by current and simultaneously determining the value Ψ of the magnetic flux associated with the secondary winding as defined in Eq. (5) [17, 19].

$$L_{\mu d} = \frac{\partial \Psi}{\partial i}. \tag{4}$$

$$\Psi = \int_S \vec{B} \cdot d\vec{S}. \tag{5}$$

In the transformer short-circuit state, and in the absence of a magnetic shunt, that is when the shunt is completely removed, the flux generated by the primary winding is almost entirely compensated in the core by the flux of the secondary winding. Introducing a shunt into the transformer window allows part of the flux to flow through it. Fig. 7 shows the division of the simulated flux into two parts, one closing its path through the magnetic shunt and the other associated with the shorted secondary winding. The amount of flux flowing through the shunt depends on the ratio of the equivalent reluctance of the path associated with the shunt (magnetic shunt and two air gaps) and the path containing the secondary winding. The value of the resultant reluctance of the magnetic circuit path (branch) with the shunt is affected not only by the position of the shunt, but also by the intensity of the current in the transformer windings. Larger current values cause the magnetic shunt to saturate, which forms part of the gap–shunt–gap branch in the transformer magnetic circuit. This results in an increase in the equivalent reluctance of this branch, and therefore reduces the flux flowing through it. This also results in less energy stored in the gap between the core and the shunt. Both the change in the position of the shunt and the current intensity translate into a nonlinear characteristic of the leakage inductance and the mutual inductance [4, 10].

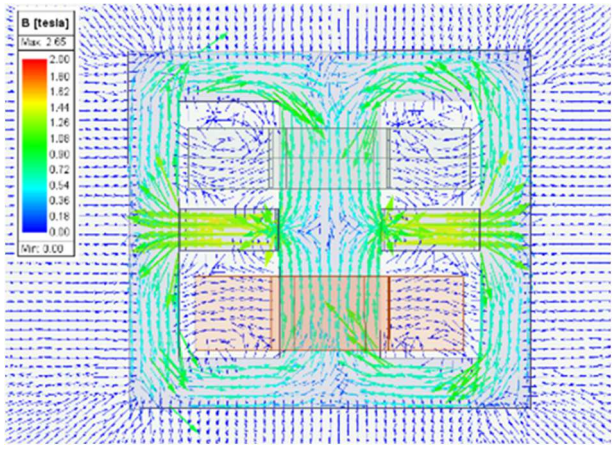

Fig. 7. Direction of the magnetic flux in the analyzed transformer.

The magnetic field distribution was analyzed assuming an ampere-turn balance between the primary and secondary windings. The excitation current of the primary winding was varied from 1A to 41A at various magnetic shunt positions, adjusted from 0mm to 180mm.

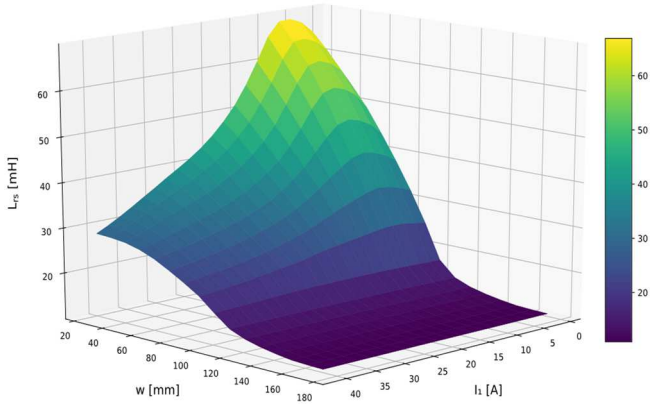

Fig. 8. Calculated static leakage inductance of the transformer primary winding.

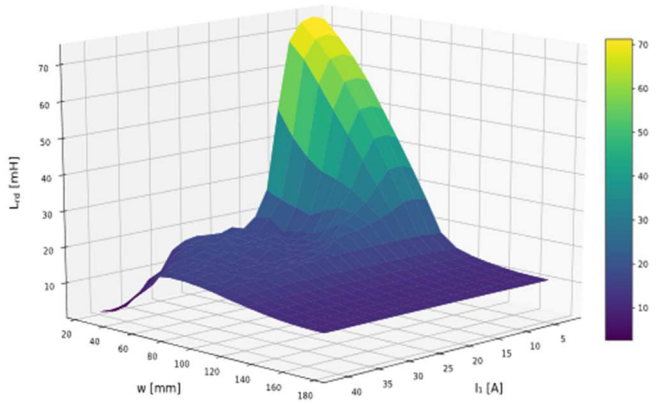

Fig. 9. Calculated dynamic leakage inductance of the transformer secondary winding.

Using the magnetic field distribution defined by Eq. (2) and Eq. (3), the static and dynamic leakage inductances associated with the primary winding were determined, as illustrated in Fig. 8 and Fig. 9. Assuming the equality of the ampere-turns of the transformer coils, the dynamic leakage inductance associated with the secondary winding is $(N_2/N_1)^2$ times smaller. Fig. 10 presents the histogram of the calculated dynamic mutual inductance values, referred to the transformer's primary side, obtained from the simulation results.

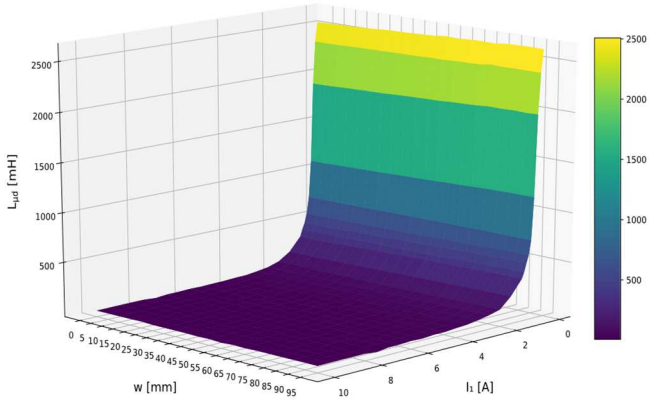

Fig. 10. Characteristic of the dynamic mutual inductance versus current excitation and the magnetic shunt extraction from the transformer window.

Measurement verification of the field model was performed by comparing the calculated and measured leakage reactance, as shown in Fig. 11.

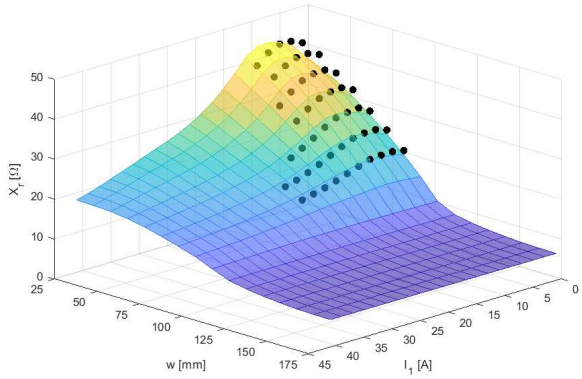

Fig. 11. Comparison between calculated and measured leakage reactance

3. FIELD-CIRCUIT MODEL FOR SIMULATION OF TRANSIENTS IN A TRANSFORMER WITH MOVABLE MAGNETIC SHUNT

The differential equations describing the operation of a single-phase transformer with a movable magnetic shunt were derived using the Lagrange formalism (Eq. 6), based on the T-shape equivalent circuit of a two-winding transformer, as shown in Fig. 12, [20]. This approach significantly simplifies the analysis, as the equivalent circuit assumes magnetic decoupling of the coils. Thus, the inductance of the individual coils will be affected only by the current flowing through the given coil [21, 22].

$$\frac{d}{dt}\left(\frac{\partial \mathcal{L}}{\partial \dot{q}_j}\right) - \frac{\partial \mathcal{L}}{\partial q_j} + \frac{\partial P}{\partial q_j} = f_j \,. \qquad (6)$$

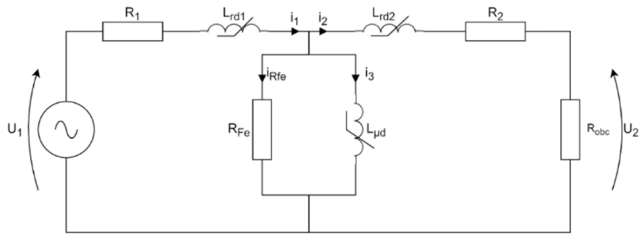

Fig. 12. T-type transformer equivalent circuit loaded with resistance R_{load}.

In the case of a transformer with a movable magnetic shunt, the value of the magnetic flux is a function dependent on both the current intensity and the position of the magnetic shunt relative to the transformer window. In the following equations, "w" denotes the retraction of the shunt from the transformer window. The generalized variables are the currents associated with the circuit branches. The equations (7), (8), and (9)

respectively describe the kinetic energy, potential energy, and heat losses due to resistances in the equivalent circuit [21, 22].

$$E_k = \int_0^{\dot{q}_1} \Psi_1(\dot{\tilde{q}}_1, w)\, d\dot{q}_1 + \int_0^{\dot{q}_2} \Psi_2(\dot{\tilde{q}}_2, w)\, d\dot{q}_2 + \int_0^{\dot{q}_3} \Psi_3(\dot{\tilde{q}}_3, w)\, d\dot{q}_3. \quad (7)$$

$$E_P = 0. \quad (8)$$

$$E_R = \frac{1}{2} R_1 \dot{q}_1^2 + \frac{1}{2} \dot{q}_2^2 (R_2 + R_{obc}) + \frac{1}{2} R_{Fe} (\dot{q}_1 - \dot{q}_2 - \dot{q}_3)^2. \quad (9)$$

After calculating the time derivatives (denoted by the dots above their letters) in the preceding expressions, we obtain the second-order derivatives system Eq. (10).

$$\begin{cases} \ddot{q}_1 = \frac{U_1 - R_1 \dot{q}_1 - R_{Fe}(\dot{q}_1 - \dot{q}_2 - \dot{q}_3)}{\boldsymbol{L}_{rd1}(\dot{q}_1)} \\ \ddot{q}_2 = \frac{-\dot{q}_2(R_2 + R_{obc}) + R_{Fe}(\dot{q}_1 - \dot{q}_2 - \dot{q}_3)}{\boldsymbol{L}_{rd2}(\dot{q}_2)} \\ \ddot{q}_3 = \frac{R_{Fe}(\dot{q}_1 - \dot{q}_2 - \dot{q}_3)}{\boldsymbol{L}_{\mu d}(\dot{q}_3)} \end{cases} \quad (10)$$

Due to a very slowly movable shunt, the velocity $\partial w / \partial t$ was assumed to be zero. During the simulation, the derivatives of the magnetic flux Ψ_j with respect to the shunt position w were not considered. It reduces the term described by Eq. 11 to zero.

$$\frac{\partial}{\partial w}\left(\Psi_j(\dot{q}_j, w)\right) \cdot \frac{\partial w}{\partial t}. \quad (11)$$

Dynamic leakage inductances, determined from magnetic field analysis, are represented in matrix form and are written in bold font in Eq. (10).

Fig. 13 shows the proposed model created in the Simulink package of MATLAB. The "Load" block contains four load variants, the three arc models described in the next chapter, and a constant resistive load.

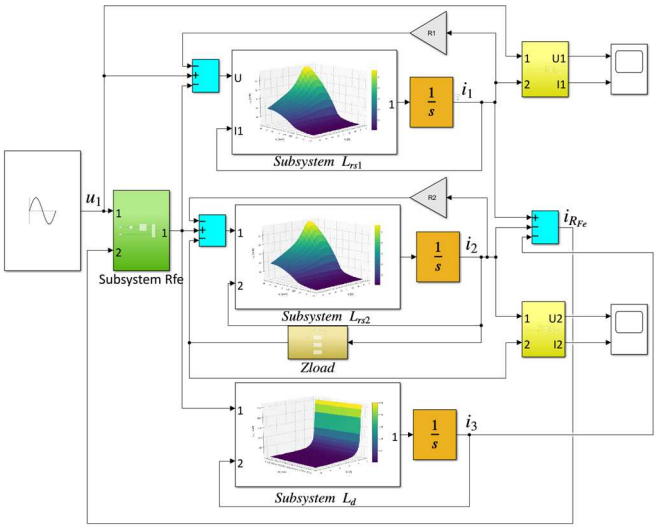

Fig. 13. Circuit model of the analyzed transformer within MATLAB/Simulink.

Based on the presented simulation model, the influence of the shunt position and the supply voltage on the output current I_2 is shown in Fig. 14. At the rated voltage, the output current varies from 50 A to 120 A.

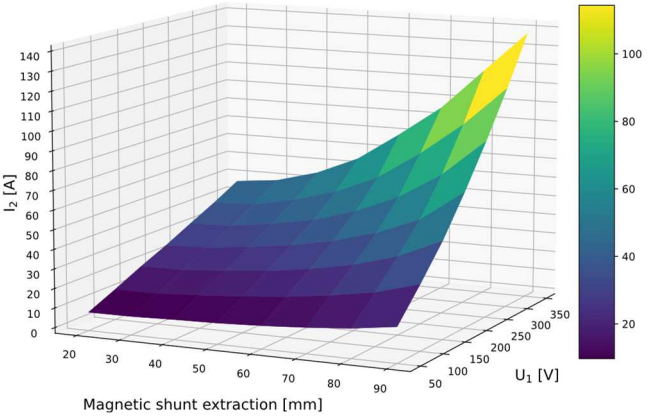

Fig. 14. Transformer secondary winding current I_2 as a function of the magnetic shunt position relative to the transformer window and the voltage supply U_1.

4. EXPERIMENTAL VERIFICATION

The simulation of transients enables the evaluation of key parameters, such as transient-state duration, the initial peak of the current wave, and the stabilized RMS values of voltage and current. The accurate simulation of all these parameters is complex; thus, a reasonably close estimation of them helps in selecting transformer protection settings or implementing the above parameters. The model proposed in this paper was validated by comparing the simulated waveforms of current and voltage with measurements obtained from a real object. The comparisons were made for the transformer's short-circuit condition. Fig. 15 shows example waveforms of the primary-side voltage and current, as well as the secondary-side current, for one position of the magnetic shunt, with an RMS supply voltage of 350V.

Good agreement between the measured and simulated results was observed for the transient state, as well as for the RMS current on both the primary and secondary sides of the transformer in the steady state. The simulated peak inrush current is about 30% higher than the measured value, which, given the many simplifications in the model, is considered acceptable.

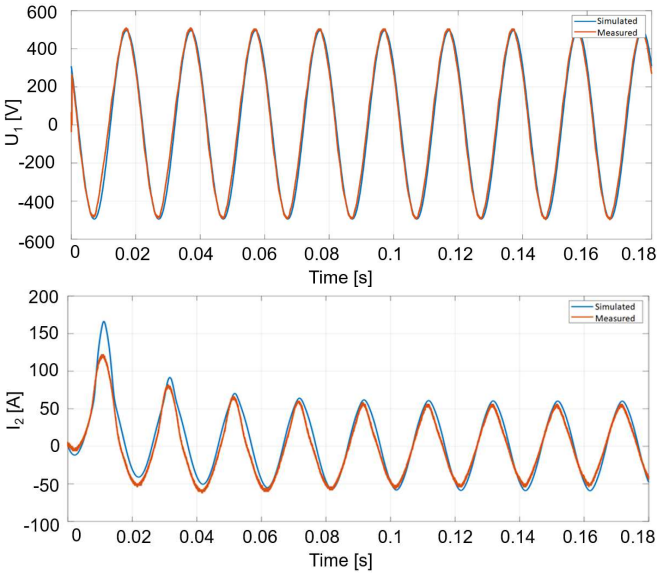

Fig. 15. Waveforms with a U_1=350V supply voltage and the magnetic shunt extraction w=25 mm from the transformer window.

The results presented in Fig. 15 were experimentally validated using the laboratory setup shown in Fig. 16. The experimental arrangement comprised an autotransformer, the transformer under investigation (Fig. 17), and measuring instruments, including a voltmeter, ammeters, and a wattmeter.

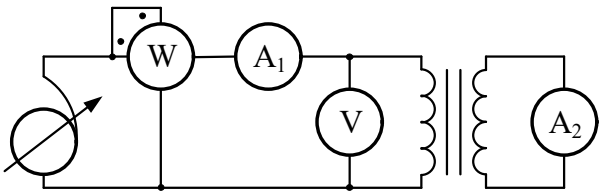

Fig. 16. The laboratory setup

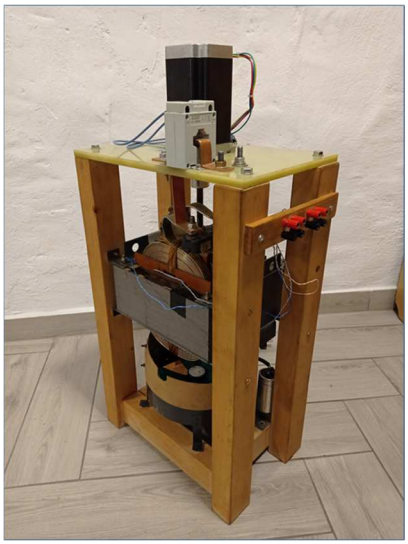

Fig. 17. Photo of the laboratory stand with the investigated transformer

5. TRANSIENT SIMULATIONS

To test the proposed hybrid field-circuit model developed in this study for its effectiveness in simulating dynamic waveforms, the electric arc simulation models were employed as the load.

Over the years, many models of electric arcs have been developed. The most widely accepted models for theoretical analysis are those proposed by Cassie (Eq. 12) and Mayr (Eq. 13). This article also analyzed the Habedank model (Eq. 14), which was derived by serially connecting the elements from the Cassie and Mayr models [23].

$$\frac{dg}{dt} = \frac{1}{\tau}\left(\frac{i_{arc} \cdot u_{arc}}{{U_c}^2} - g\right). \tag{12}$$

where: g – arc electrical conductivity [S], τ – time constant [s], u_{arc} – instantaneous voltage drop across the arc [V], i_{arc} – instantaneous current flowing through the arc [A], U_c – arc voltage (constant parameter) [V].

$$\frac{dg}{dt} = \frac{1}{\tau}\left(\frac{g^2 \cdot u_{arc}^2}{P_0} - g\right). \tag{13}$$

where: P_0 – power delivered by the arc [W].

In a stable electric arc, the following expression holds $P_0 = i_{arc} \cdot u_{arc}$, where the product $i_{arc} \cdot u_{arc}$ represents the instantaneous power of the electric arc. By comparing the models described by equations (12) and (13), it is possible to identify the conditions under which the constant parameters of the models must be determined. For a range of small values of arc current, P_0 takes a continuous value (as in Mayr's model). In contrast, in the region of large current values, the relation $P_0 = g \cdot U_C$ applies, (Cassie's model), [24].

$$\begin{cases} \frac{dg_C}{dt} = \frac{1}{\tau_C}\left(\frac{(u_{arc}g_C)^2}{{U_c}^2 g_c} - g_C\right) \\ \frac{dg_M}{dt} = \frac{1}{\tau_M}\left(\frac{(u_{arc}g_C)^2}{P_0} - g_M\right). \\ \frac{1}{g} = \frac{1}{g_M} + \frac{1}{g_C} \end{cases} \quad (14)$$

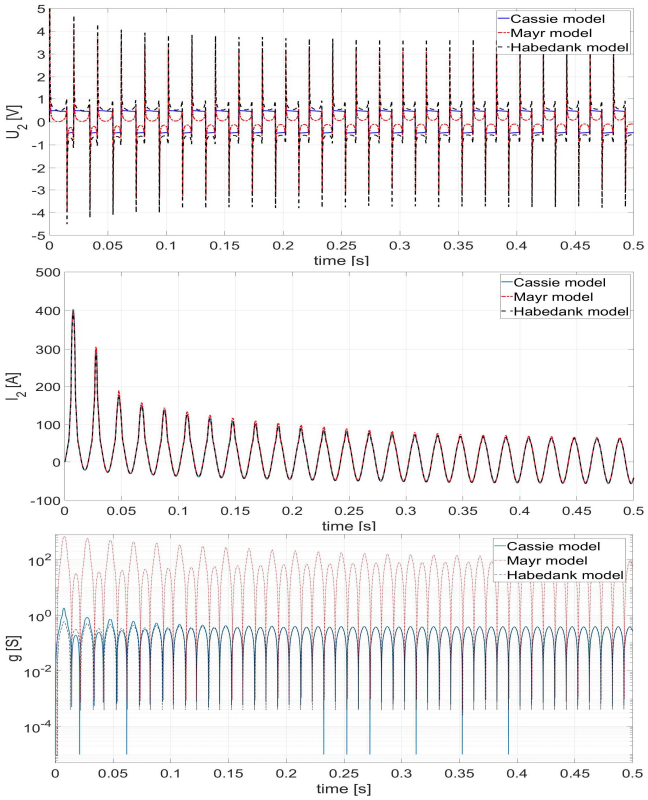

Fig. 18. Simulation of the voltage and current intensity waves and impedance of an electric arc at the supply voltage U_1=350V and the magnetic shunt extraction w=25 mm.

Figures 18 and 19 show the time waveforms of voltages, currents, and electric arc impedance for two different positions of the magnetic shunt. The waveforms are plotted for the three electric arc models presented above. To increase the clarity of the impedance values, the impedance scale is shown on a logarithmic axis. It can be seen that there is good agreement in the time waveforms of voltages and currents across simulations for various arc models.

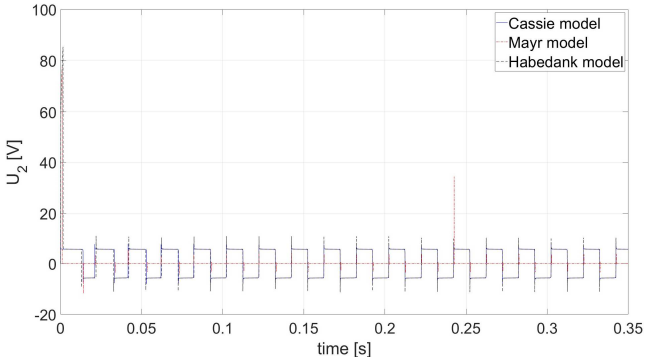

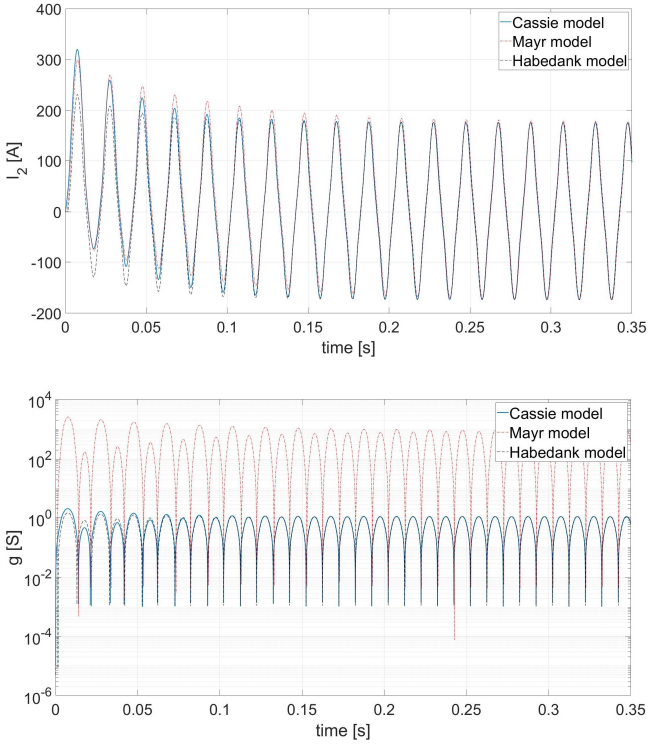

Fig. 19. Simulation of time courses and impedance of an electric arc at a supply voltage U_1 equal to 350 V and a shunt extraction from the transformer window equal to 85 mm.

6. SUMMARY

Determining the transformer integral parameters from magnetic field distribution analysis enables simulation of dynamic waveforms using the hybrid field-circuit model proposed in this paper, which accounts for magnetic shunt position changes and transformer voltage supply. Aside from its usefulness, such an approach has some advantages: it is simple and easy to interpret, although simulations may be affected by modeling errors. Good agreement between the measured time waveforms and the simulated values for a resistive load, obtained during the measurement verification, confirmed the correctness of the model developed in this paper. The proposed hybrid field-circuit model therefore enables accurate simulation of dynamic voltages and currents for both linear and nonlinear loads, including electric arcs. It was observed that nonlinear loads result in a higher peak inrush current and a longer duration of transient states than in a simulation with a constant load. This paper also confirms that the magnetic shunt enables accurate operation over a wide range for both static and nonlinear loads. The difference between the simulated and measured peak inrush current values shown in Fig. 14 suggests that additional phenomena should be included in the mathematical model. However, it is almost impossible to create a transformer model that accounts for all physical phenomena, as transformer analysis spans numerous fields of science, including electromagnetism, thermodynamics, mechanics, and acoustics. In addition, analysis of such a model would be very time-consuming, making a fully comprehensive model almost impractical. Therefore, mathematical models are created under certain assumptions, omitting some phenomena. Considering

hysteresis loops and eddy currents during simulation can improve the accuracy of the proposed mathematical model, especially for transformers with a core and a magnetic shunt made of non-oriented steel.

The advantage of the proposed model is a significant reduction in the simulation time when the system load changes. The analysis of the time-stepping field-circuit model of the transformer studied in the paper for each load condition would require multi-hour simulations. In contrast, the proposed hybrid model allows results to be obtained in just a few seconds. It's worth noting that the magnetic shunt's position relative to the transformer window significantly alters the object's parameters, requiring further simulations.

The rapid development of the electrical power grid, driven by the diversification of power sources, has led to the incorporation of numerous new power electronic devices into the system. In light of this, the proposed model could be effectively used for simulating a complex electrical grid, where transformers are merely one of an ever-growing number of components.

REFERENCES

[1] E. Palmgren and T. Rasa, "Modelling roles of mathematics in physics," *Science & Education*, vol. 33, pp. 365-382, 2022, doi: 10.1007/s11191-022-00393-5.

[2] Y. Liu, R. Wu and A. Yang, "Research on medical problems based on mathematical models," *Mathematics*, vol. 11, no. 13, art. 2842, 2023, doi: 10.3390/math11132842.

[3] V. Mokhov, S. Aliukov, A. Alabugin, and K. Osintsev, "A review of mathematical models of macroeconomics, microeconomics, and government regulation of the economy," *Mathematics*, vol. 11, no. 14, art. 3246, 2023, doi: 10.3390/math11143246.

[4] B. Tomczuk and D. Weber, "Effect of magnetic shunts on shell-type transformers characteristics," *Energies*, vol. 16, no. 19, art. 6814, 2023, doi: 10.3390/en16196814.

[5] K. Dawood, M. A. Cinar, B. Alboyaci, and O. Sonmez, "A new method for the calculation of leakage reactance in power transformers," *J. Electr. Eng. Technol.*, vol. 12, pp. 1883–1890, 2017, doi: 10.5370/JEET.2017.12.5.1883.

[6] E. Mechkov, R. Tzeneva, V. Mateev, and I. Yatchev, "Thermal analysis using 3D FEM model of oil-immersed distribution transformer," in *Proc. 19th Int. Symp. Electrical Apparatus and Technologies (SIELA)*, Bourgas, Bulgaria, May 2016.

[7] ANSYS Maxwell 3D User's Guide, ANSYS Inc. [Online]. Available: www.ansys.com. [Accessed: Jan. 7, 2024].

[8] S. V. Kulkarni and S. A. Khaparde, *Transformer Engineering: Design, Technology, and Diagnostics*, 2nd ed. Boca Raton, FL, USA: CRC Press, 2012.

[9] B. Tomczuk, "Analysis of 3-D magnetic fields in high leakage reactance transformers," *IEEE Trans. Magn.*, vol. 30, pp. 2734–2738, 1994.

[10] B. Tomczuk, D. Weber, and D. Wajnert, "Shunt regulation analysis of the short-circuit inductance based on 3D magnetic field in high reactance transformer with movable shunt," *Przegląd Elektrotechniczny*, vol. 95, pp. 31–34, 2019.

[11] B. S. Alves, P. Kuo-Peng, and P. Dular, "Contribution to power transformers leakage reactance calculation using analytical approach," *Int. J. Electr. Power Energy Syst.*, vol. 105, pp. 470–477, 2019.

[12] G. B. Kumbhar and S. V. Kulkarni, "A directly coupled field-circuit model of a transformer to study surge phenomena and for frequency response analysis," in *Proc. 18th National Power Systems Conf. (NPSC)*, Guwahati, India, 2014, pp. 1–5, doi: 10.1109/NPSC.2014.7103838.

[13] B. Tomczuk, D. Koteras, J. Zimon, and A. Waindok, "Calculation of the transient currents in transformers using field-circuits methods," *Przegląd Elektrotechniczny*, vol. 87, pp. 126–130, 2011.

[14] A. Rashwan, A. I. M. Ali, and T. Senjyu, "Current stress minimization for isolated dual active bridge DC–DC converter," *Sci. Rep.*, vol. 12, art. 16980, 2022, doi: 10.1038/s41598-022-21359-1.

[15] J. K. Sykulski, *Computational Magnetics*. London, U.K.: Chapman & Hall, 1995.

[16] B. Tomczuk and D. Koteras, "Magnetic flux distribution in amorphous modular transformers," *J. Magn. Magn. Mater.*, vol. 323, pp. 1611–1615, 2011.

[17] H. F. Farahani, M. Zare, S. Mohammad, P. Razi, and A. Khodakarami, "Finite element analysis of leakage inductance of 3-phase shell-type and core-type transformers," *Res. J. Appl. Sci. Eng. Technol.*, vol. 4, pp. 1721–1728, 2012.

[18] B. Bandelier and F. Rioux-Damidau, "Mixed finite element method for magnetostatics in $\mathbb{R}^3$," *IEEE Trans. Magn.*, vol. 34, pp. 2473–2476, 1998.

[19] K. J. Binns, P. J. Lawrenson, and C. W. Trowbridge, *The Analytical and Numerical Solution of Electric and Magnetic Fields*. New York, NY, USA: Wiley, 1993.

[20] A. Nogueira, "Calculation of power transformers equivalent circuit parameters using numerical field solutions," *Int. J. Res. Rev. Appl. Sci.*, vol. 17, no. 1, pp. 113–121, 2013.

[21] A. Hemeida *et al.*, "Magnetic Equivalent Circuit and Lagrange Interpolation Function Modeling of Induction Machines Under Broken Bar Faults," *IEEE Trans. Magn.*, vol. 59, no. 12, pp. 1–5, 2023, doi: 10.1109/TMAG.2023.3306207.

[22] Z. Biolek, D. Biolek, and V. Biolková, "Lagrangian for circuits with higher-order elements," *Entropy*, vol. 21, no. 11, art. 1059, 2019, doi: 10.3390/e21111059.

[23] H. Haraldsson, Y. A. Tesfahunegn, M. Tangstad, and G. Sævarsdottir, "Modelling of electric arcs for industrial applications: A review," in *Proc. INFACON XVI*, 2021. doi: 10.2139/ssrn.3927158.

[24] X. Li, C. Pan, D. Luo, and Y. Sun, "Series DC arc simulation of photovoltaic system based on Habedank model," *Energies*, vol. 13, no. 6, art. 1416, 2020, doi: 10.3390/en13061416.